


Article

Employing the Defective Photonic Crystal Composed of Nanocomposite Superconducting Material in Detection of Cancerous Brain Tumors Biosensor: Computational Study

C. Malek ¹, M. Al-Dossari ^{2,3}, S. K. Awasthi ⁴, Z. S. Matar ⁵, N. S. Abd El-Gawaad ⁶, Walied Sabra ¹ and Arafa H. Aly ^{1,*} 

¹ TH-PPM Group, Physics Department, Faculty of Sciences, Beni-Suef University, Beni Suef 62514, Egypt

² Physics Department, King Khalid University, Dhahran Aljanoub, Abha 61421, Saudi Arabia

³ Research Center for Advanced Materials Science (RCAMS), King Khalid University, Abha 61413, Saudi Arabia

⁴ Department of Physics and Material Science and Engineering, Jaypee Institute of Information Technology, Noida 201304, India

⁵ Department of Physics, Faculty of Applied Science, Umm Al-Qura University, Mecca 24382, Saudi Arabia

⁶ Physics Department, King Khalid University, Mohayel Asser, Abha 61421, Saudi Arabia

* Correspondence: arafa.hussien@science.bsu.edu.eg



Citation: Malek, C.; Al-Dossari, M.; Awasthi, S.K.; Matar, Z.S.; Abd El-Gawaad, N.S.; Sabra, W.; Aly, A.H. Employing the Defective Photonic Crystal Composed of Nanocomposite Superconducting Material in Detection of Cancerous Brain Tumors Biosensor: Computational Study. *Crystals* **2022**, *12*, 540. <https://doi.org/10.3390/cryst12040540>

Academic Editors: Muhammad Ali Butt and Svetlana Nikolaevna Khonina

Received: 22 March 2022

Accepted: 7 April 2022

Published: 12 April 2022

Publisher's Note: MDPI stays neutral with regard to jurisdictional claims in published maps and institutional affiliations.



Copyright: © 2022 by the authors. Licensee MDPI, Basel, Switzerland. This article is an open access article distributed under the terms and conditions of the Creative Commons Attribution (CC BY) license (<https://creativecommons.org/licenses/by/4.0/>).

Abstract: The present research is focused on the externally tunable defect mode properties of a one dimensional (1D) defective photonic crystal (DPhC) for fast detection of cancerous brain tumors. The proposed design has utilized conventional 1D DPhC whose cavity is coated with SiO₂ nanoparticles embedded in a superconducting material layer called a nanocomposite layer. The purpose of a nanocomposite superconducting layer is to induce temperature dependent external tuning of the defect mode inside PBG, in addition, to changing in the angle of incidence. The inclusion of a nanocomposite layer also improves the interaction between light and different brain tissue samples under examination. In order to investigate the transmission properties of the proposed structure the transfer matrix formulation in addition to the MATLAB computational tool has been used. First, we have chosen the optimized internal parameters at normal incidence to obtain the maximum performance of the design. Secondly, the effect of change in angle of incidence has been studied to further increase the performance by means of sensitivity, quality factor, the figure of merit and limit of detection to ensure external tuning of defect mode. After achieving a maximum value of sensitivity (4139.24 nm/RIU) corresponding to a sample containing a wall of brain tissues at $\theta = 63^\circ$ we have further investigated the effect of change in temperature of nanocomposite layers on the position and intensity both of the defect mode inside PBG. We have found that the increase in temperature results in minute changes in sensitivity but a significant increase in the intensity of defect mode which is highly required in any photonic biosensing design. The findings of this study may be very useful for designing various bio-sensing structures which could have a significant and decisive role in the field of biomedical applications.

Keywords: photonic crystals; superconducting material; biosensors; TMM; sensitivity

1. Introduction

The development of rapid, point of care and timely diagnostic technologies for cancerous cells is a promising research field. The unwanted growth of cells anywhere in the human body may become the root cause of malignancy. In 2018 around 19 million new cancer cases and 10 million deaths due to cancer have been reported as per the study by the international society which monitors cancer. Most of these demises were due to untimely diagnosis of cancer [1,2]. Therefore, it is an essential requirement to develop near patient, cost effective and accurate testing facilities. Recently photonic technology based biosensors have emerged as a potential candidate for label free, rapid and accurate detection of malignant

tissues which causes cancer in the human body. These biosensors are capable of detecting minute changes in the refractive index of the sample under consideration [3–8]. The sensing mechanism of exhaled breath to detect the presence of toluene traces in the human body has been studied [9] with the help of a 1D photonic crystal (PhC). The results of this study may be helpful for the diagnosis of lung cancer. Actually, organs of the human body are made up of cells of a specific refractive index. For example, the refractive index variation of cells of different parts of the human brain is between 1.3 to 1.42 due to changes in the concentration of protein levels inside cells [10]. The malignant cells which are responsible for cancerous brain tumors have a large amount of water content than normal cells [11]. This excess water results in higher dielectric constant and electrical conductivity values of cancerous cells and hence, the refractive index of cancerous cells is more than normal cells. The brain is one of the most sophisticated and important organs controlling all the real and virtual functions of our body and it is very difficult as well as costly to examine cancerous brain tumors with the help of existing conventional cancer diagnostic technologies [12–15]. A lot of studies have been carried out for rapid, accurate and cost effective detection of cancer cells, as well as other diseases in the human body. For example, Nejad et al. reported a metamaterial based tunable and supersensitive biosensor composed of split ring resonators which could detect various cancer cells in the infrared wavelength region. The sensitivity of this structure varies between 633 nm/RIU to 658 nm/RIU [11]. A surface plasmon resonance based PhC fiber biosensor was studied by Yasli for early stage detection of cancer cells belonging to various parts of the body except for the brain [14]. Recently Panda et al. studied a graphene based 1D PhC biosensor capable of real time examination of cancers cells. This design could achieve a sensitivity of 290 nm/RIU only [8]. Auguie et al. investigated Tamm plasmon (TP) resonance dependent biosensing applications of 1D PhC based on theoretical simulations which were verified experimentally [16]. In addition, TP resonance based gas sensing applications of 1D PhCs have been theoretically examined by Zaky et al. [17]. They obtained ultra high sensitivity of value 5018 nm/RIU. In addition, they studied the hemoglobin detection strategy employing surface plasmon resonance with high quality factor and figure of merit. A novel way of detecting tuberculosis by using 1D DPhC is studied by Arafa et al. [18]. By keeping all the technological aspects involved in the timely detection of cancerous brain tumors by employing several photonic biosensors, in this study we have proposed a photonic biosensor capable of detecting cancerous brain tumors with extremely high sensitivity.

In the present piece of research work, we have proposed a simple 1D DPhC design for the timely detection of various malignant tissues and cells of the human brain. The purpose of this study is to detect malignant brain tissues so that their rapid growth may be prevented to save the life of the sufferer. The proposed design utilizes the conventional 1D DPhC associated with a nanocomposite superconducting material coated cavity of air. The different samples under investigation are infiltrated into the cavity one by one to obtain the desired results. To the best of our knowledge, a 1D DPhC whose cavity is coated with nanocomposite material has been rarely used for the accurate detection of brain tumors. The normal and cancerous cells are infiltrated into the cavity using refractive index miniaturization sensing applications to obtain enhanced sensitivity from the design. The transmission spectra have been computed by using the transfer matrix method (TMM).

2. Biosensor Design

The proposed 1D DPhC $(AB)^N CDC(AB)^N$ capable of detecting cancerous brain tissues is depicted in Figure 1. Here, A and B represent alternating layers of two identical 1D PhCs $(AB)^N$ of period N used in the design. These two PhCs are joined together through air cavity D coated with nanocomposite material C as depicted in Figure 1. The cerebrospinal fluid (CSF) samples containing different brain tissues extracted from various parts of the human brain through a long needle have been injected into the cavity region of the structure to perform investigations as per requirement. The process of collecting samples from the human brain is called a lumbar puncture [1,2].

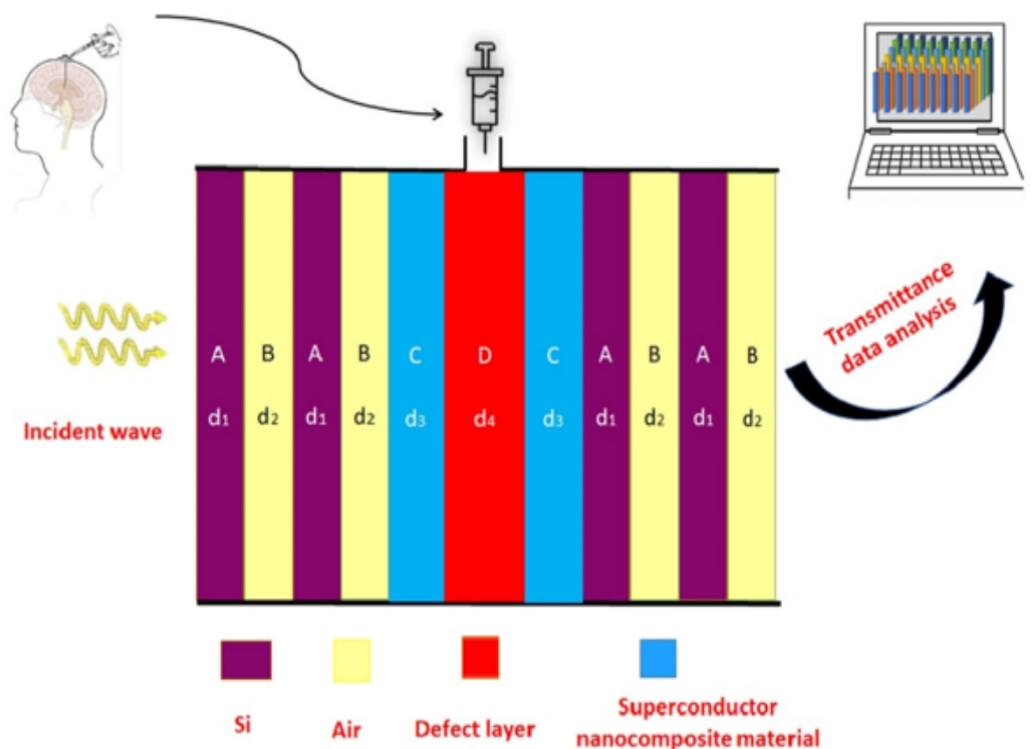


Figure 1. The schematic architecture of the proposed biosensing structure $(AB)^N CDC(AB)^N$. The fluids containing different brain tissues extracted from various parts of human brain through a long needle have been injected into the cavity region marked with red color through inlet valve mounted on top of the structure.

3. Theoretical Formulation of the Problem

The symbols n_1 , n_2 and d_1 , d_2 represented the refractive index (RI) and thickness of layers A and B, respectively, of 1D PhC $(AB)^N$ used in the structure $(AB)^N CDC(AB)^N$. The refractive index and thickness of nanocomposite superconducting layers C of material $YBa_2 Cu_3 O_7$ are denoted by n_3 and d_3 , respectively. The air cavity D of thickness d_4 is to be used to examine various brain tissue samples. The period thickness of 1D PhC $(AB)^N$ is given $dd = d_1 + d_2$. The refractive index of various samples under investigation is being denoted by n_4 .

The two-fluid model describes the refractive index of high temperature superconductor $YBa_2 Cu_3 O_7$ as [19–21]

$$n_{sc} = \sqrt{1 - \frac{c^2}{\omega^2 \lambda_L^2}} \quad (1)$$

where c , ω and λ_L are representing velocity of incident light in free space, angular frequency of the incident light and the temperature-dependent London penetration depth, respectively. The expression of temperature-dependent London penetration depth is given as [21,22]

$$\lambda_L(T) = \frac{\lambda_o}{\sqrt{1 - \left(\frac{T}{T_c}\right)^2}} \quad (2)$$

Here λ_o is the London penetration depth at $T = 0$ K and T_c is the critical temperature of the superconductor material.

The refractive index n_3 of nanocomposite superconductor material is defined with the help of the Maxwell-Garnett formula as [23,24]

$$n_3 = \sqrt{\epsilon_{eff}} = \sqrt{\frac{\epsilon_m (2\eta\epsilon_{sc} - 2\eta\epsilon_m + \epsilon_{sc} + 2\epsilon_{sc})}{(2\epsilon_m + \epsilon_{sc} + \eta\epsilon_m - \eta\epsilon_{sc})}} \quad (3)$$

where ϵ_m is the permittivity of the dielectric material SiO_2 , $\epsilon_{sc}()$ is the permittivity of high temperature superconductor material $\text{YBa}_2\text{Cu}_3\text{O}_7$ and η is representing the volume fraction of SiO_2 material embedded into $\text{YBa}_2\text{Cu}_3\text{O}_7$. The effective permittivity of the nanocomposite layer is denoted as ϵ_{eff} .

The transfer matrix representing the j th (=A, B, C and D) layer of the proposed design at an angle θ is given [25–27]

$$M_j = \begin{pmatrix} \cos \gamma_j & -\frac{i}{p_j} \sin \gamma_j \\ -ip_j \sin \gamma_j & \cos \gamma_j \end{pmatrix} \quad (4)$$

The value of p_j of j th layer is $p_j = z_0 n_j \cos \theta_j$ and $p_j = \frac{\cos \theta_j}{z_0 n_j}$ for TE and TM polarized light waves, respectively. Here, $\gamma_j = \frac{2\pi}{\lambda_0} n_j d_j \cos \theta_j$ with d_j , n_j and θ_j are representing the thickness, refractive index and ray angle of light inside the j th layer of the structure. The free space impedance and wavelength are represented by z_0 and λ_0 , respectively. The total transfer matrix of the whole structure can be obtained by using Equation (4) as

$$M_T = (X_A X_B)^N X_D X_D X_D (X_A X_B)^N \\ = \begin{pmatrix} M_{11} & M_{12} \\ M_{21} & M_{22} \end{pmatrix} \quad (5)$$

Here, M_{11} , M_{12} , M_{21} and M_{22} are representing elements of total transfer matrix M_T . The coefficient of transmission t is given by

$$t = \frac{2\eta_0}{(M_{11} + M_{12}\eta_S)\eta_0 + (M_{21} + M_{22}\eta_S)} \quad (6)$$

For TE and TM polarized light waves the values of η_0 and η_S representing incident and exit medium, respectively are given as $\eta_0 = z_0 n_0 \cos \theta_0$, $\eta_S = z_0 n_S \cos \theta_S$ and

$$\eta_0 = \frac{\cos \theta_0}{z_0 n_0}, \quad \eta_S = \frac{\cos \theta_S}{z_0 n_S} \quad (7)$$

The transmittance (T) of the design $(AB)^N \text{CDC} (AB)^N$ can be obtained as [28–30]

$$T = \frac{\eta_S}{\eta_0} |t|^2 \quad (8)$$

4. Results and Discussions

The present research work highlights the bio-sensing capabilities of the proposed 1D DPhC based on the interaction of light and the structure. The proposed structure $(AB)^N \text{CDC} (AB)^N$ is made up of two 1D binary PCs $(AB)^N$ of a similar kind. The dielectric material Si in association with air has been chosen to represent the A and B layers of both 1D binary PCs $(AB)^N$, respectively. The refractive index of Si and air layers of the design has been fixed to $n_1 = 3.3$ and $n_2 = 1$, respectively. On the other hand, the thickness of the Si and air layers of the structure have been optimized to $d_1 = 0.35 \mu\text{m}$ and $d_2 = 0.275 \mu\text{m}$, respectively, to obtain a wider PBG which is one of the essential requirements of designing any 1D photonic biosensors. Next, we are introducing the details of the design of the cavity region which will be used to examine different analytes in this manuscript. The cavity

region of the design is composed of two identical thin buffer layers of thickness d_3 which are associated together through an air cavity of a thickness of d_4 . The two identical buffer layers are made up of the nanocomposite high temperature superconducting material $\text{YBa}_2\text{Cu}_3\text{O}_7$ in which the dielectric material SiO_2 is embedded to obtain an engineered nanocomposite superconducting material. The thickness of both the nanocomposite buffer layers has been set to $0.09\ \mu\text{m}$. The refractive index of the nanocomposite buffer layer is dependent upon wavelength and governed by Equation (3). We have chosen the thickness of the cavity region such that $d_4 = dd = d_1 + d_2$, where dd is the length of the period of the 1D PhC $(AB)^N$. We have fixed the period N of both the 1D PhCs $(AB)^N$ used in this design as 2 to minimize the length of the design. The London penetration depth (λ_0) at temperature $T = 0\ \text{K}$ of the nanocomposite high superconductor layers is set to $200\ \text{nm}$. The numeric values of critical temperature (T_c) and volume fraction (η) of the nanocomposite layer are set to $92\ \text{K}$ and 0.8 , respectively. The permittivity of the SiO_2 material layer is taken as 2.1025 [4]. In this simulation work, we have chosen air as a surrounding medium and substrate of the design. The purpose of selecting nanocomposite buffer layers to design this structure is due to the unique applications of nanocomposite materials which enable the development of a variety of biophotonic sensing applications on the basis of refractive index sensing mechanisms of various fluids provided by metal or dielectric nanoparticles. Moreover, the inclusion of nanocomposite buffer layers also increases external parameters, such as T of superconducting layers by which we can control the bio-sensing performance of the design externally. In this simulation work, we have studied the externally tunable bio-sensing performance of the proposed design dependent upon the angle of incidence (θ) and ambient temperature (T) of the nanocomposite superconducting material layer.

In recent years, the refractive index analysis of various kinds of body fluids containing normal and abnormal cells has become important for improving the operation of plasmonics and photonics-based bio-sensing applications. Photonic bio-sensing has emerged as a powerful tool in detection, monitoring and drug designing to accelerate the diagnostic technologies involved in rapid disease detection due to economic, accurate and highly sensitive results. This research work has been given attention to investigating the various brain lesion samples to find any kind of malignancy inside the human brain with the help of 1D DPhC. Actually damaged brain tissues which are localized inside the brain may result in brain tumors and are classified as brain lesions. The unwanted growth of these brain lesions may become the root cause for the development of malignant brain tumors and are fatal for the patient if not diagnosed on time. The lumbar puncture or spinal tap are the two common procedures to collect samples by injecting a thin and long needle through the skull or spinal cord of the affected person. The human brain floats in a colorless fluid called Cerebrospinal fluid (CSF). This fluid ensures all the requirements to various parts of the human brain as well as the spinal cord are met, and also filters the waste from those places. The patient having symptoms of autoimmune diseases, inflammation in the spinal cord and/or brain tissues or leukemia may be due to some viral or bacterial infections inside the brain so CSF investigation may become essential as per the advice of a doctor. Since it is a well-established fact that the refractive index of CSF of a healthy person is 1.3333 in the infrared region of the electromagnetic spectrum, we have taken this value of the refractive index as an internal reference to carry out the findings of the proposed work [31].

The threshold value of the refractive index of CSF containing various brain lesions which determines the malignancy in different samples containing brain lesions is 1.395 . This threshold value is very helpful in identifying the malignancy in the examination of different samples containing various brain lesions. If the refractive index of the sample under investigation is less or equal to 1.395 the sample is nonmalignant otherwise the sample is said to be malignant due to excess water content inside malignant cells. Actually, our design relocates the position of defect mode side the PBG of the structure depending upon the change in the refractive index of different brain tissues in the samples under investigation. Thus, by measuring the separation between positions of modified defect

mode with respect to defect mode associated with the CSF sample, one can find malignancy in the sample. The refractive index values of different samples containing normal and damaged brain tissues used in this study have been mentioned by Biswas, T. [31]. The change in the level of proteins inside brain tissues is responsible for the corresponding change in the RI of various brain tissues.

In order to carry out investigations pertaining to this research, we have infiltrated the cavity region of our 1D DPhC structure $(AB)^2CDC(AB)^2$ with different samples containing brain tissues as per the information given by Biswas, T. [31], separately to identify the nature of the malignancy in these samples. For achieving the objective of the proposed work we have studied the transmission spectra of 1D DPhC structure $(AB)^2CDC(AB)^2$ dependent on two external factors, first, change in incident angle and the second change in the ambient temperature of nanocomposite superconducting material layer. The research has been conducted in the infrared region of the electromagnetic spectrum which extends from 3.2 μm to 4.7 μm . Figure 2 depicts the transmission spectra of proposed biosensor $(AB)^2CDC(AB)^2$ at a normal incidence with $d_4 = 15dd$ and $\eta = 0.8$. It shows ten distinguishable defect mode peaks centered at different positions inside PBG which extends from 4.15 μm to 4.7 μm corresponding to ten separate samples containing different brain tissues as per the details given by Biswas, T. [31]. The intensity of these peaks gradually varies between 65% to 45% corresponding to samples containing brain tissues separately from CSF to lymphoma, respectively. The intensity of these defect modes is sufficient to be detected by spectrometer through optical fiber into a computer with the help of software. The larger refractive index contrast between silicon and air layers of the 1D DPhC results in a wider PBG width of 0.6 μm . The change in the analyte into the cavity region from CSF to Lymphoma as given by Biswas, T. [31] one by one results in the movement of defect mode inside PBG towards a higher wavelength with a gradual decrease in the intensity of the respective defect mode as shown in Figure 2. This shifting of defect mode inside PBG is measured with reference to the position of defect mode corresponding to the CSF sample. The standing wave formulation inside the laser cavity can be used to justify the movement of defect mode inside PBG as given in Equation (9). The change in the refractive index of the analyte under investigation alters the resonant condition which governs laser radiation from the cavity by fixing the optical path difference inside the laser cavity.

$$\Delta = p\lambda = n_{\text{eff}}Z \quad (9)$$

In order to represent the optical path difference between standing waves inside the laser cavity, an integer, central wavelength of defect mode, effective refractive index of the cavity and geometrical path difference we have used notations Δ , p , λ , Z and n_{eff} , respectively.

We have evaluated the performance of the proposed design capable of sensing various samples containing different brain tissues with the help of one of the most popular parameters known as sensitivity (S) of the structure. It determines the minute shift in the central wavelength of defect mode due to the corresponding change in the refractive index of various analytes involved in the investigation. Basically, it helps to estimate the minute sensing capabilities of the biosensors which is defined as [28–33]

$$S = \frac{\delta\lambda}{\delta n} \quad (10)$$

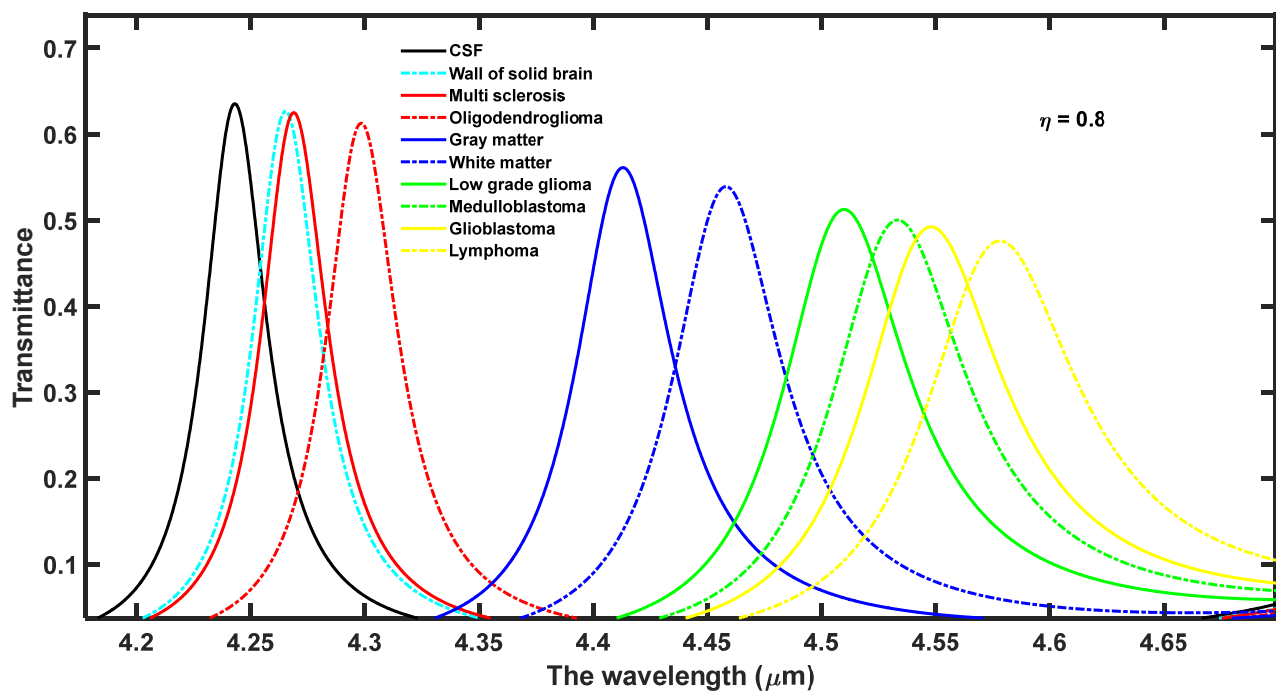


Figure 2. The transmittance spectra of 1D DPhC $(AB)^2CDC(AB)^2$ when cavity is loaded with ten different brain tissues one by one at normal incidence with $d_4 = 15dd$ and $\eta = 0.8$.

Here, the change in the refractive index of the sample under investigation and the resulting shift in the position of the central wavelength of the defect mode inside the PBG are represented by δn and $\delta\lambda$, respectively. We have used the CSF sample as a reference to calculate the S of the proposed design. This calculation has been implemented by loading the cavity of the design one by one with different samples containing various brain tissues. The central wavelength of defect mode of wavelength (λ_d) and sensitivity (S) of the structure with of cavity thickness $d_4 = 15dd$ and volume fraction of a nanocomposite layer $\eta = 0.8$ at $\theta = 0^\circ$ is being summarized in Table 1 corresponding to different samples containing brain tissues one by one.

Table 1. The refractive index (RI), central wavelength of defect mode (λ_d) and sensitivity (S) of the proposed design with $d_4 = 15dd$ and $\eta = 0.8$ under the influence of different samples containing brain tissues at $\theta = 0^\circ$.

Brain Tissues	RI	λ_d (μm)	S ($\mu\text{m}/\text{RIU}$)
CSF	1.3333	4.2431	
Wall of solid brain	1.3412	4.2651	2.78481
Multi sclerosis	1.3425	4.2689	2.80434
Oligod-endroglioma	1.3531	4.298	2.77272
Gray matter	1.3951	4.4128	2.74595
White matter	1.4121	4.4579	2.72588
Low grade glioma	1.4320	4.5099	2.70314
Medulloblastoma	1.4412	4.5331	2.68767
Glioblastoma	1.4470	4.5487	2.68777
Lymphoma	1.4591	4.5779	2.66136

From the data mentioned in Table 1, it can be observed that the S of the structure varies between the maximum value of 2.80434 $\mu\text{m}/\text{RIU}$ to the minimum value of 2.66136 $\mu\text{m}/\text{RIU}$ when the cavity is loaded separately with samples containing multiple sclerosis to lymphoma brain tissues, respectively. Now we extend this study further to improve the sensitivity of the design by tuning the external parameters of the design, such as angle of

incidence and temperature of nanocomposite high superconductor layer keeping all other internal parameters constant as discussed above.

4.1. The Effect of Increasing the Angle of Incidence on the Performance of the Design

In this section, the effect of increasing the angle of incidence from 0° to 63° has been observed on the performance of the proposed 1D DPhC $(AB)^2CDC(AB)^2$. For this purpose the transmission spectra of the proposed design corresponding to different incident angles at $\theta = 10^\circ$, $\theta = 20^\circ$, $\theta = 30^\circ$, $\theta = 40^\circ$, $\theta = 50^\circ$, $\theta = 60^\circ$ and $\theta = 63^\circ$ have been plotted in Figure 3a–g, respectively. Here, the ambient temperature of the nanocomposite layer has been fixed to $T = 4.5$ K.

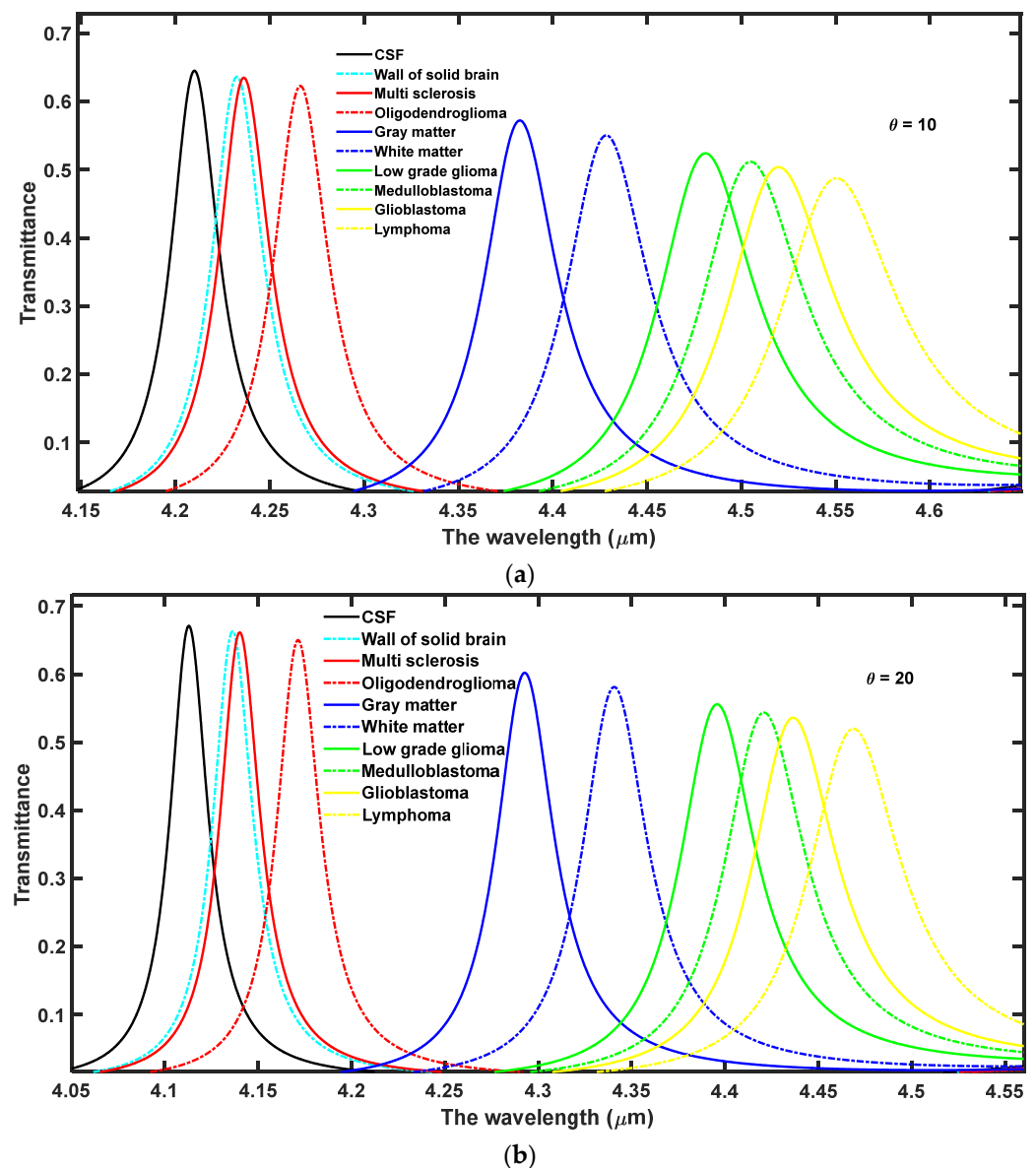


Figure 3. Cont.

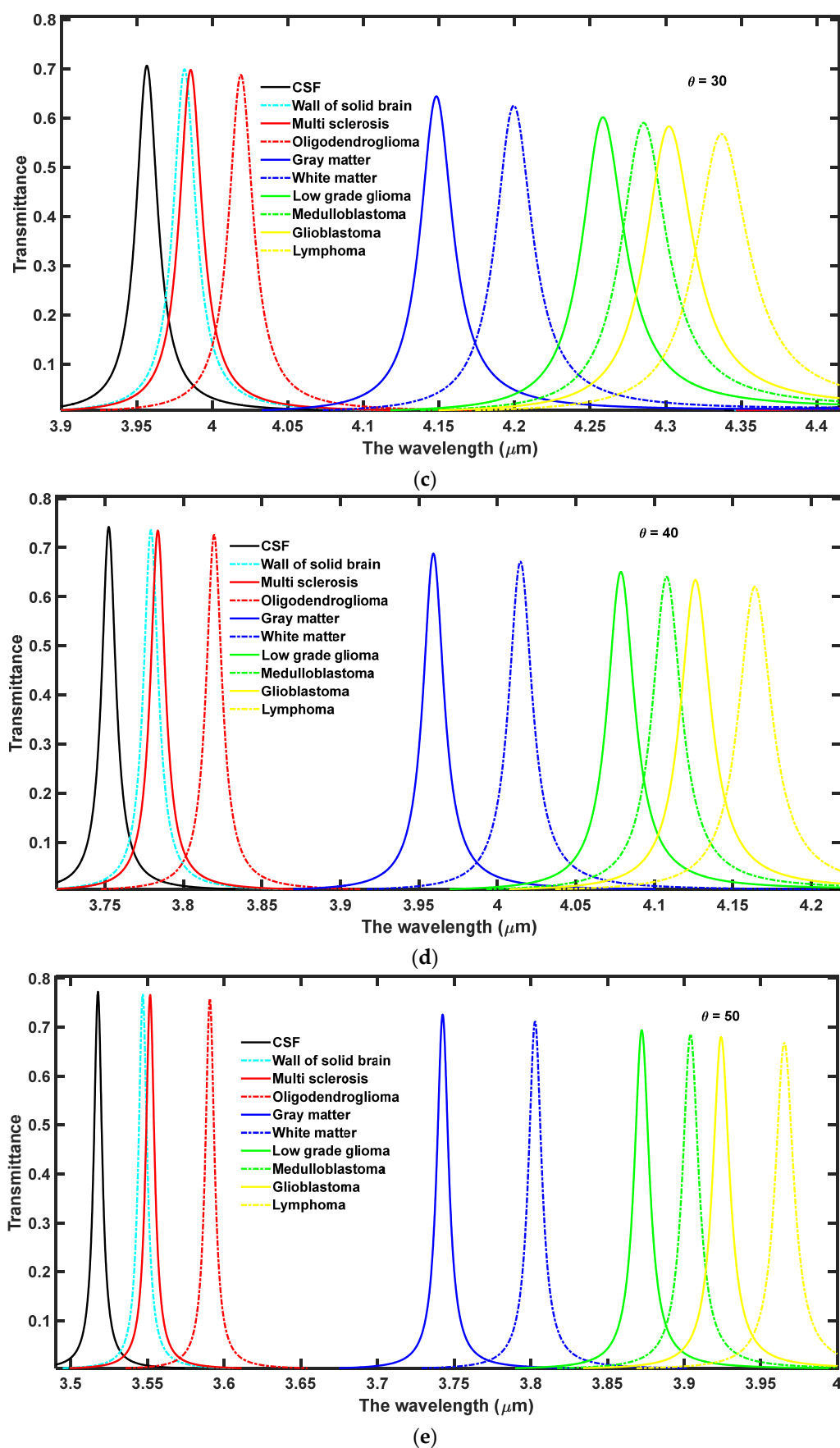


Figure 3. Cont.

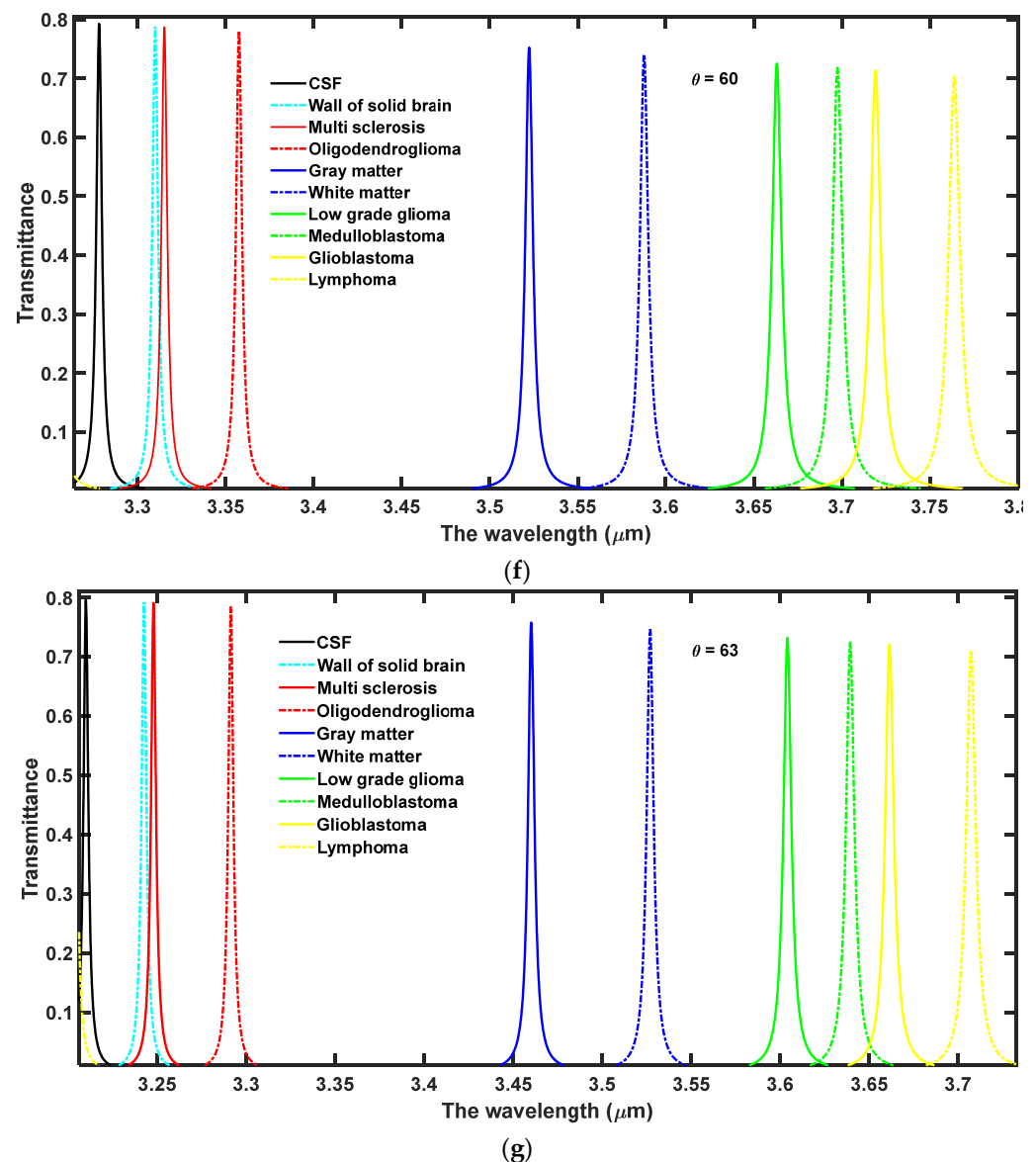


Figure 3. The transmittance spectra of 1D DPhC $(AB)^2CDC(AB)^2$ infiltrated with ten different samples containing brain tissues with $d_4 = 15dd$ and $\eta = 0.8$ corresponding to oblique incidence at (a) $\theta = 10^\circ$, (b) $\theta = 20^\circ$, (c) $\theta = 30^\circ$, (d) $\theta = 40^\circ$, (e) $\theta = 50^\circ$, (f) $\theta = 60^\circ$ and (g) $\theta = 63^\circ$.

As evident from Figure 3 the increase in the angle of incidence from 0° to 63° results in the blue shift of defect modes associated with each sample. Moreover, this increase in incident angle also reduces the full-width half maximum (FWHM) of each resonant mode inside PBG which in turn improves the intensity of each defect mode by fulfilling the law of conservation of energy. Actually due to an increase in the angle of incidence the energy associated with each defect mode remains constant inside PBG. The optimum value of angle of incidence has been found to be $\theta = 63^\circ$ at which the sensitivity of the proposed design varies between the maximum value of $4.13924 \mu\text{m}/\text{RIU}$ to the minimum value of $3.9523 \mu\text{m}/\text{RIU}$ corresponding to samples containing a wall of the solid brain to lymphoma brain tissues, respectively. Thus the increase in the incident angle results in a significant improvement in the sensitivity of the proposed structure in contrast to the results of Figure 2 at $\theta = 0^\circ$. The increase in the angle of incident improves the interaction between the sample under investigation and light. This interaction improves the resonance between the standing waves inside the cavity region which results in the reduction of FWHM with an enhanced intensity of defect mode associated with each sample containing different

brain tissues. Thus, by increasing the incident angle one can improve the performance of the proposed design composed of 1D DPhCs. The angle dependent sensitivity and central wavelength of defect modes associated with samples containing various brain tissues separately are summarized in Table 2. The pictorial representation in three-dimensional bar graph of the data presented in Table 2 is shown in Figure 4 below.

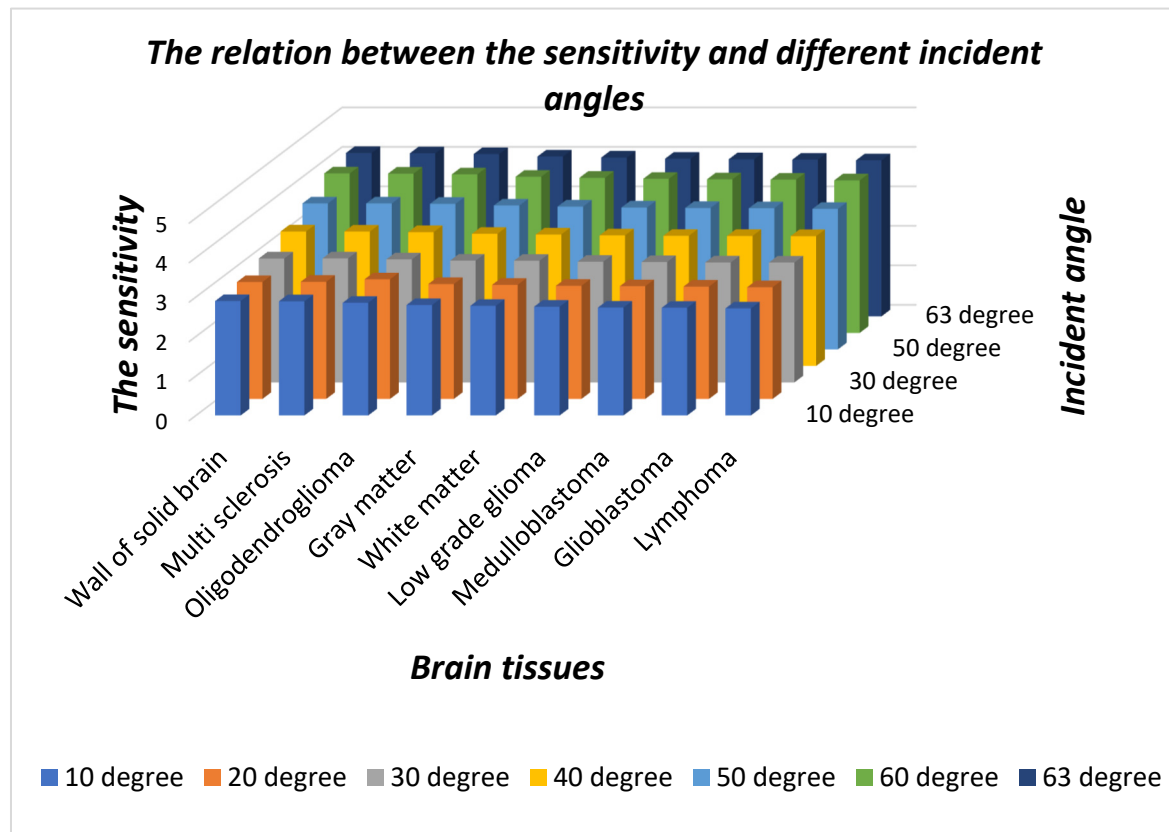


Figure 4. The 3D bar graph showing incident angle dependent sensitivity of the proposed 1D DPhC $(AB)^2CDC(AB)^2$ infiltrated with nine different samples containing brain tissues with respect to CSF sample with $d_4 = 15dd$, $\eta = 0.8$ at $T = 4.5$ K.

Figure 4 shows the sensitivity of the proposed design dependent upon different incident angles under the influence of nine samples of different brain tissues with respect to the sample containing nonmalignant CSF brain tissue. It is evident from the figure that as the incident angle increases it improves the sensitivity of the design because of improved interaction between light and the sample under investigation. The sensitivity of the structure loaded with different samples is almost stagnant at a particular incident angle. Thus, for designing any high performance photonic biosensor, we should focus our attention to obtain the optimum value of incident angle which corresponds to maximum sensitivity. In this study, we have limited the optimum value of incident angle to 63° which corresponds to sensitivity variation between the maximum value of $4.13924 \mu\text{m}/\text{RIU}$ to the minimum value of $3.9523 \mu\text{m}/\text{RIU}$ corresponding to a wall of the solid brain to lymphoma brain tissue samples, respectively. Besides this, the minimum size of the structure has also been achieved by fixing the period number to 2 which makes the fabrication of the design easier and cheaper. This design utilizes only two material layers in addition to the air layer. In all the above mentioned findings, the maximum 80% intensity of defect mode has been achieved.

Table 2. The performance evaluation table presenting defect mode wavelength (λ_d) and sensitivity (S) of the proposed design corresponding to different incident angles as 10° , 20° , 30° , 40° , 50° , 60° and 63° when the cavity is infiltrated with ten samples containing different brain tissues.

Brain Tissues	RI	$\theta = 10^\circ$		$\theta = 20^\circ$		$\theta = 30^\circ$		$\theta = 40^\circ$		$\theta = 50^\circ$		$\theta = 60^\circ$		$\theta = 63^\circ$	
		λ_d (μm)	S ($\mu\text{m}/\text{RIU}$)	λ_d (μm)	S ($\mu\text{m}/\text{RIU}$)	λ_d (μm)	S ($\mu\text{m}/\text{RIU}$)	λ_d (μm)	S ($\mu\text{m}/\text{RIU}$)	λ_d (μm)	S ($\mu\text{m}/\text{RIU}$)	λ_d (μm)	S ($\mu\text{m}/\text{RIU}$)	λ_d (μm)	S ($\mu\text{m}/\text{RIU}$)
CSF	1.3333	4.2097		4.1128		3.9567		3.7524		3.5177		3.278		3.2099	
Wall of solid brain	1.3412	4.2326	2.89873	4.1362	2.96202	3.9815	3.13924	3.7793	3.40506	3.5469	3.6962	3.3099	4.03797	3.2426	4.13924
Multi- sclerosis	1.3425	4.2363	2.89130	4.1401	2.96739	3.9856	3.14130	3.7837	3.40217	3.5517	3.69565	3.3151	4.03260	3.2479	4.13043
Oligod-endroglioma	1.3531	4.2662	2.85353	4.1728	3.0303	4.0184	3.11616	3.8195	3.38888	3.5907	3.68686	3.3575	4.01515	3.2913	4.11111
Gray matter	1.3951	4.3826	2.79773	4.2927	2.9110	4.1474	3.08576	3.9592	3.34627	3.7429	3.64401	3.5224	3.95469	3.4601	4.04854
White matter	1.4121	4.4284	2.77538	4.3406	2.89086	4.1995	3.081218	4.0147	3.32868	3.8028	3.61802	3.5875	3.92766	3.5269	4.02284
Low grade glioma	1.4320	4.4816	2.75481	4.3957	2.86626	4.2585	3.05775	4.0787	3.30597	3.8724	3.59371	3.6631	3.90172	3.604	3.99290
Medulloblastoma	1.4412	4.5046	2.73308	4.4208	2.85449	4.2857	3.049119	4.1079	3.29471	3.9042	3.58202	3.6976	3.88878	3.6392	3.97868
Glioblastoma	1.4470	4.5198	2.72735	4.4364	2.84608	4.3022	3.03869	4.1267	3.29199	3.9242	3.57519	3.7192	3.88038	3.6613	3.97009
Lymphoma	1.4591	4.5507	2.71065	4.4687	2.82909	4.3387	3.03656	4.1659	3.28696	3.9654	3.55882	3.7639	3.86248	3.7071	3.9523

4.2. The Effect of Increasing the Temperature of Nanocomposite Buffer Layer on the Performance of the Design

Finally, we have studied the effects of increasing the temperature of nanocomposite buffer layers made up of the high temperature superconductor $\text{YBa}_2\text{Cu}_3\text{O}_7$, in which the dielectric material SiO_2 is embedded. The performance of our proposed structure has a cavity thickness of $d_4 = 15 \text{ dd}$, and a volume fraction of SiO_2 material embedded into the nanocomposite buffer layers $\eta = 0.8$ and at $\theta = 63^\circ$. We wish to improve the intensity of defect modes inside PBG by increasing the ambient temperature T of the buffer layers. For this purpose, we have studied the effect of increasing the ambient temperature of superconducting material layers to $T = 10 \text{ K}$, 30 K , 50 K , 70 K , and 90 K , on the transmission spectra of the proposed design loaded with different samples containing brain tissues extracted from various parts of the brain, as shown in Figure 5a–e, respectively. This range of temperature has been selected keeping the critical temperature ($T_c = 92 \text{ K}$) of the superconducting material into account. Moreover, it is the experimentally observed fact by Marel et al. that $\text{YBa}_2\text{Cu}_3\text{O}_7$ shows the critical reflectivity below T_c in the infrared region of the electromagnetic spectrum which is in agreement with the two fluid model of superconductors [31]. It has been observed that the increase in temperature results in the moderate shifting of defect modes towards higher wavelength side inside PBG. The increase in T increases λ_L , which is a function of T as evident from Equation (2) which in turn also increases the refractive index of superconducting material. Due to the increment in the refractive index value of superconductor material the refractive index contrast between the layers of the structure reduces which leads to the shifting of PBG towards the higher wavelength side. This shifting of PBG also triggers the red shifting of defect modes which are located inside PBG and are associated with different samples as evident in Figure 5. The increase in temperature also improves the transmission intensity of each defect mode associated with each sample which reaches the maximum (close to unity corresponding to all samples) at $T = 90 \text{ K}$ though the FWHM of each defect mode remains stagnant. The numeric values of the central wavelength of defect mode (λ_d), percentage transmittance of defect mode (Trans.) and sensitivity (S) of the proposed structure $(AB)^2\text{CDC}(AB)^2$ are associated with different samples containing brain tissues of various parts of the brain have been listed in Table 3 corresponding to different ambient temperatures of nanocomposite layers. Moreover, the increase in the temperature of the ambient medium of the superconducting buffer layers decreases the superconducting electrons (n_s) of the material, which in turn increases the number of normal electrons (n_e) of the superconducting material. The superconductor is transformed into normal material when the ambient temperature exceeds the critical temperature of the material due to the presence of a large number of n_e in comparison to n_s in the superconducting material. This effect has not been included in this study because the present structure will be transformed into conventional PhC and has already been discussed by many researchers working in this field.

The numeric data of Table 3 have been visualized with the help of Figures 6 and 7. Figures 6 and 7 have been plotted to depict a 3D bar graph showing temperature dependent sensitivity of the proposed design and transmittance of defect mode associated with different fluid samples containing brain tissues respectively, as per the information given in Table 3. Figure 6 shows as T increases from 10 K to 90 K in steps of 20 K , the sensitivity of the design varies between a maximum value of $4.12658 \text{ } \mu\text{m}/\text{RIU}$ to a minimum of $3.95071 \text{ } \mu\text{m}/\text{RIU}$ corresponding to a sample containing a wall of the solid brain and lymphoma brain tissues, respectively, at $T = 10 \text{ K}$. Further increases in temperature gradually reduces the sensitivity corresponding to each sample under investigation. The sensitivity variation lowers down between a maximum of $4.07594 \text{ } \mu\text{m}/\text{RIU}$ to a minimum of 3.89189 corresponding to separate samples containing walls of solid brain and lymphoma brain tissues, respectively, at $T = 90 \text{ K}$. This reduction in sensitivity is due to the increase in the number of n_e in contrast to the number of n_s with an increase in ambient temperature. It has been also noticed in Figure 6 that the sensitivity of the structure varies between

maximum to minimum values corresponding to samples containing walls of solid brain and lymphoma brain tissues, respectively, at all temperatures.

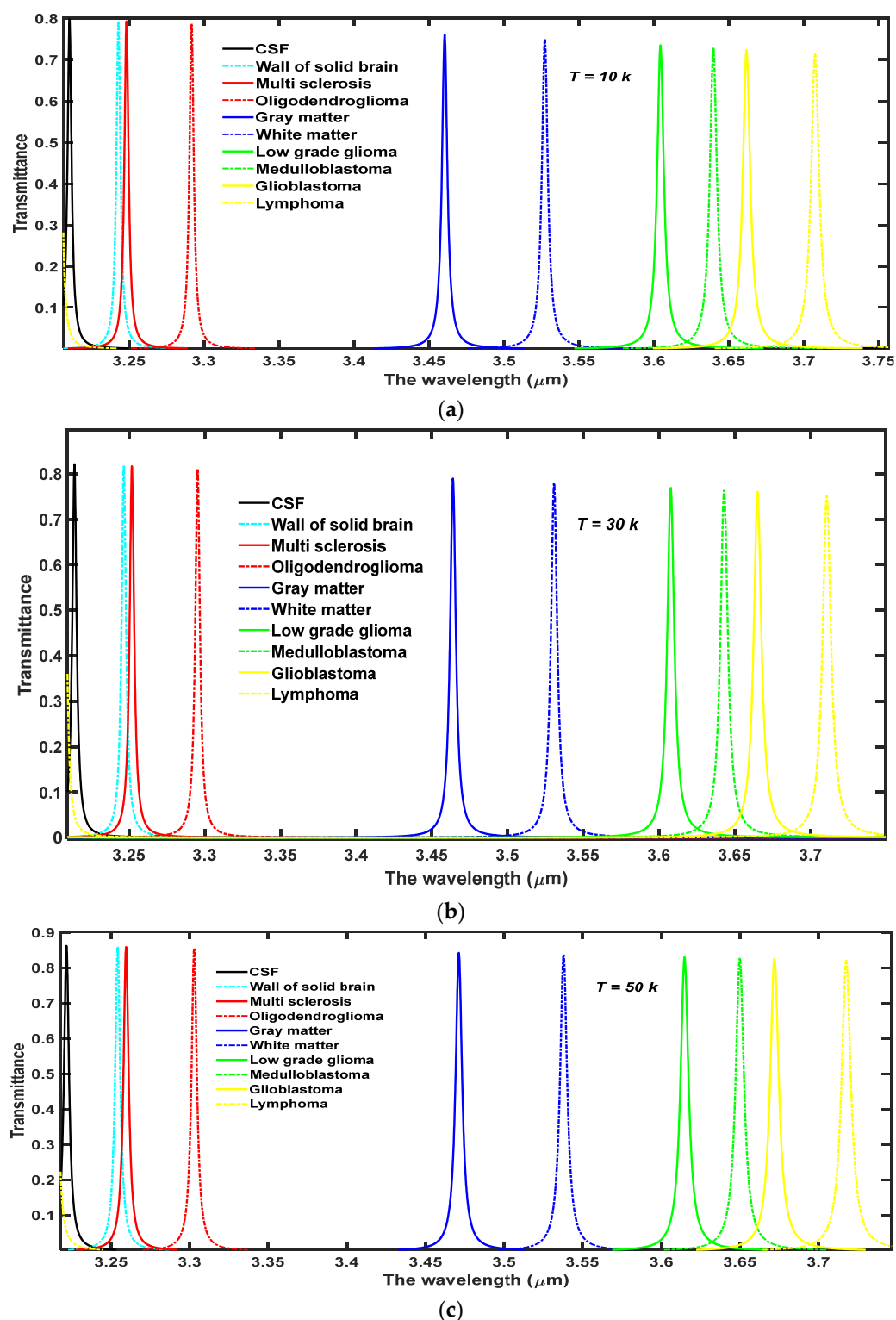


Figure 5. Cont.

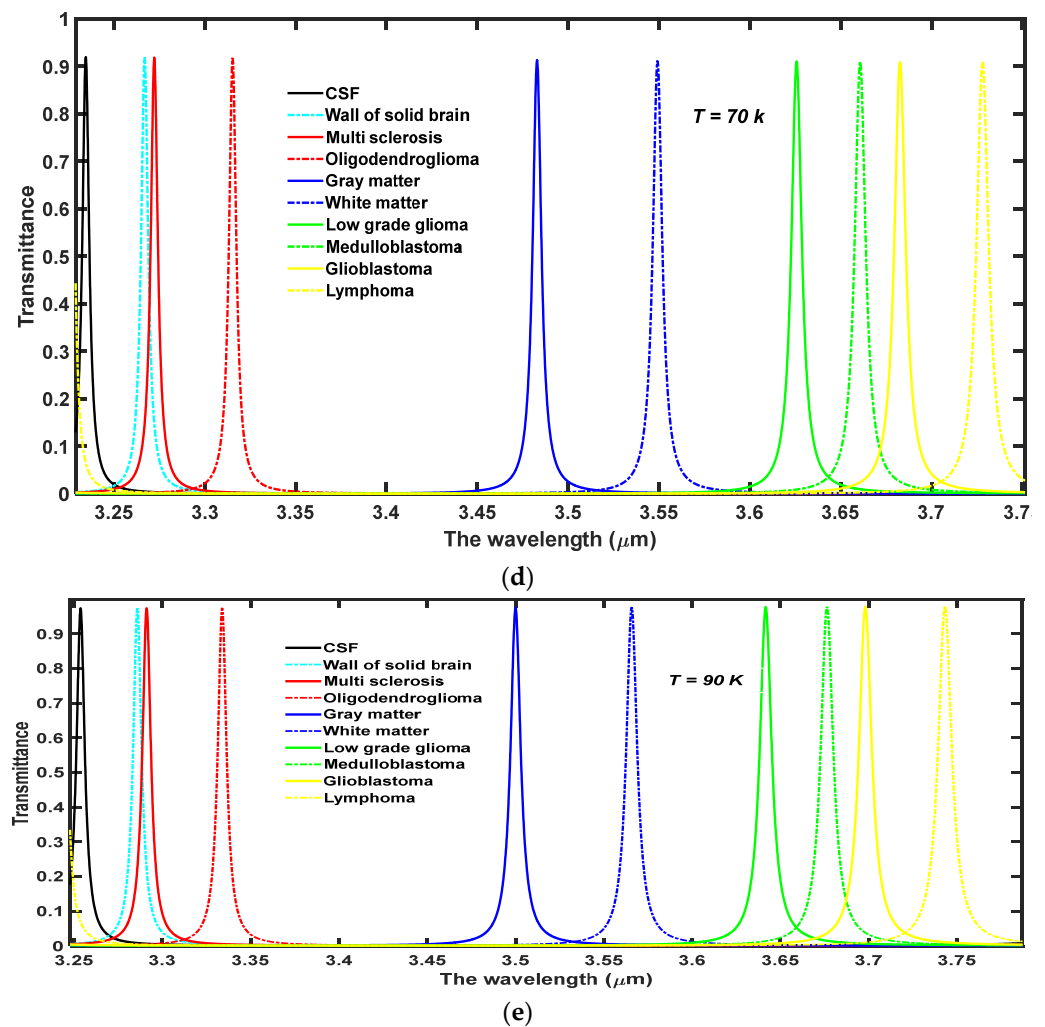


Figure 5. The temperature dependent transmittance spectra of 1D DPhC $(AB)^2CDC(AB)^2$ corresponding to $d_4 = 15dd$, $\eta = 0.8$ and $\theta = 63^\circ$. The cavity is infiltrated with ten different samples containing brain tissues. The ambient temperature (T) of nanocomposite buffer layers fabricated either side of cavity layer is fixed to (a) $T = 10$ K, (b) $T = 30$ K, (c) $T = 50$ K, (d) $T = 70$ K and (e) $T = 90$ K.

Besides this, we have also plotted a 3D bar graph in Figure 7 which shows the dependence of transmission intensity of defect modes associated with the respective samples under investigation on the temperature of the ambient medium. Figure 7 shows that transmission intensity of the defect modes varies between maximum to minimum values associated with CSF to lymphoma samples, respectively, at fixed temperatures. The increase in temperature of nanocomposite buffer layers improves the intensity of defect mode which originates due to the presence of various samples inside the cavity. The intensity reaches a maximum that is close to unity for all samples when the ambient temperature is kept at 90 K which is close to the critical value of the superconducting layer.

Table 3. The performance evaluation table showing central wavelength of defect mode (λ_d), percentage transmittance of defect mode (*Trans.*) and sensitivity (*S*) of the proposed design with $d_4 = 15dd$, $\eta = 0.8$ and $\theta = 63^\circ$ dependent upon different ambient temperatures of nanocomposite buffer layers (*T*) as 10 K, 30 K, 50 K, 70 K and 90 K when cavity is loaded with ten different samples containing brain tissues.

Brain Tissues	RI	λ_d (μm)	<i>T</i> = 10 K		λ_d (μm)	<i>T</i> = 30 K		λ_d (μm)	<i>T</i> = 50 K		λ_d (μm)	<i>T</i> = 70 K		λ_d (μm)	<i>T</i> = 90 K	
			Trans. (%)	<i>S</i> ($\mu\text{m}/\text{RIU}$)		Trans. (%)	<i>S</i> ($\mu\text{m}/\text{RIU}$)		Trans. (%)	<i>S</i> $\mu\text{m}/\text{RIU}$		Trans. (%)	<i>S</i> ($\mu\text{m}/\text{RIU}$)		Trans. (%)	<i>S</i> ($\mu\text{m}/\text{RIU}$)
CSF	1.3333	3.2103	0.795	—	3.214	0.82	—	3.2218	0.863	—	3.2345	0.919	—	3.2536	0.9736	—
Wall of solid brain	1.3412	3.2429	0.794	4.12658	3.2466	0.817	4.12658	3.2543	0.861	4.11392	3.2669	0.9184	4.10126	3.2858	0.9738	4.07594
Multi sclerosis	1.3425	3.2482	0.792	4.11956	3.2519	0.816	4.11956	3.2597	0.86	4.11956	3.2722	0.9183	4.09782	3.2909	0.971	4.05434
Oligodendroglioma	1.3531	3.2917	0.787	4.11111	3.2953	0.809	4.10606	3.303	0.857	4.10101	3.3154	0.917	4.08585	3.3338	0.974	4.0505
Gray matter	1.3951	3.4604	0.76	4.04692	3.4639	0.788	4.04368	3.4712	0.843	4.03559	3.4829	0.913	4.01941	3.5	0.975	3.98705
White matter	1.4121	3.5272	0.749	4.02157	3.5307	0.78	4.01903	3.5378	0.838	4.01015	3.5492	0.911	3.99365	3.5657	0.976	3.96065
Low grade glioma	1.432	3.6043	0.735	3.99189	3.6077	0.769	3.98885	3.6147	0.831	3.98074	3.6258	0.91	3.96453	3.6416	0.977	3.9311
Medulloblastoma	1.4412	3.6394	0.728	3.97683	3.6429	0.763	3.97497	3.6498	0.828	3.96663	3.6608	0.909	3.95088	3.6763	0.9776	3.91751
Glioblastoma	1.447	3.6617	0.724	3.97009	3.665	0.76	3.96657	3.6719	0.827	3.95866	3.6826	0.908	3.94107	3.6981	0.9781	3.90941
Lymphoma	1.4591	3.7073	0.714	3.95071	3.7107	0.752	3.94833	3.7175	0.822	3.94038	3.7284	0.903	3.92607	3.7432	0.9787	3.89189

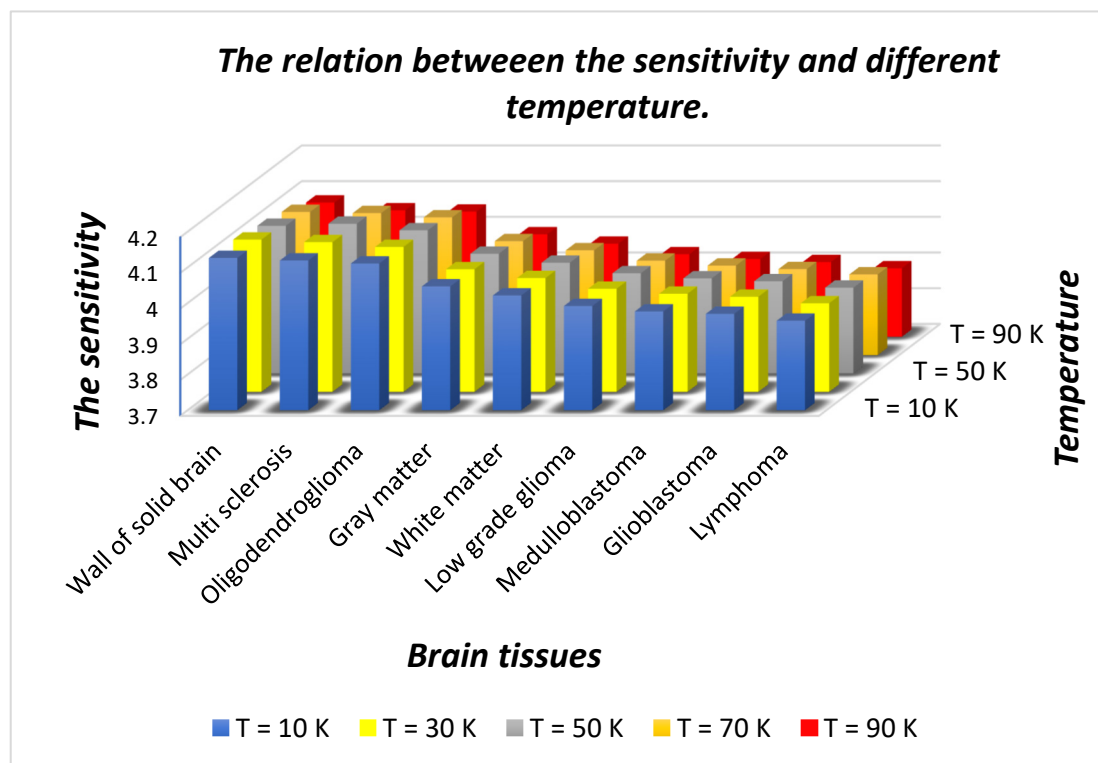


Figure 6. The 3D bar graph showing temperature dependent sensitivity of the proposed 1D $DPhC(AB)^2CDC(AB)^2$ when the cavity is loaded with nine different samples containing brain tissues at $d_4 = 15dd$, $\eta = 0.8$ and $\theta = 63^\circ$ corresponding to different values of ambient temperature.

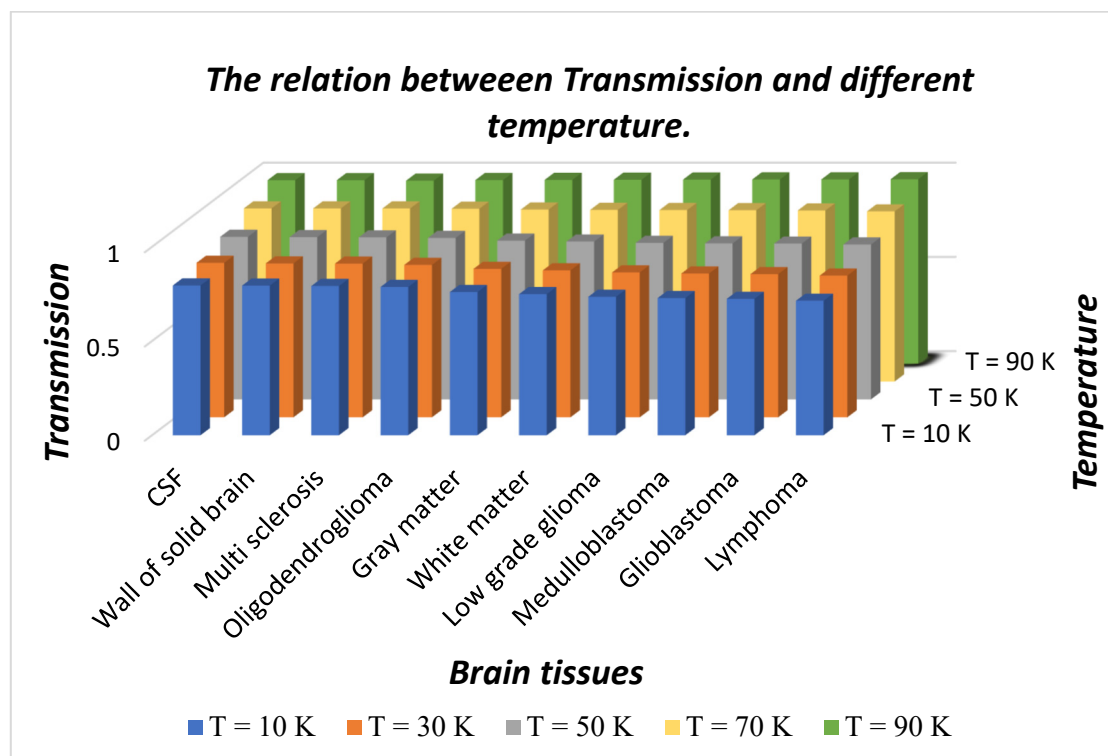


Figure 7. The 3D bar graph showing temperature dependent transmittance of defect mode originates due to presence of different samples inside cavity one by one at $d_4 = 15dd$, $\eta = 0.8$ and $\theta = 63^\circ$. The ambient temperature varies between 10 K to 90 K.

4.3. The Evaluation of Bio-Sensing Performance of the Proposed Design

In this section of the manuscript, we have analyzed the bio-sensing performance of the proposed design with the help of various parameters as listed in Table 4. For the fulfillment of our goal we have calculated the numeric values of parameters *FWHM*, quality factor (*Q*), figure of merit (*FoM*) and limit of detection (*LoD*) associated with the design under optimum conditions which are already discussed in Sections 4.1 and 4.2 in addition to the sensitivity of the design. The optimum conditions are very helpful to ensure the maximum performance of the design. We have used the standard definitions defined in references [32,33] for calculating the numeric values of parameters *FWHM*, *Q*, *FoM* and *LoD* associated with our structure. The various parameters evaluating the performance of the proposed design under optimum conditions with $d_4 = 15dd$, $\eta = 0.8$, $\theta = 63^\circ$ and $T = 50$ K have been summarized in Table 4. The sensitivity of the design varies between a maximum value of 4139.241 nm/RIU to a minimum value of 3952.305 nm/RIU corresponding to sample wall of the solid brain to lymphoma, respectively. The average value of the sensitivity of the design is 4038. Furthermore, our design also possesses reasonably high quality factor and figure of merit values of order 10^3 which makes our design suitable for sensitive detection of cancerous brain tumors. The order of limit of detection of our design is 10^{-5} which is extremely low. The low value of the limit of detection is one of the desirable requirements for designing any biosensor. It signifies the smallest change in the refractive index of the sample under investigation which can be detected accurately.

Table 4. The numeric values of parameters central wavelength of defect mode (λ_d), FWHM, sensitivity (*S*), quality factor (*Q*), figure of merit (*FoM*) and limit of detection (*LoD*) associated with our biosensor $(AB)^2CDC(AB)^2$ under optimum condition which describe the performance.

Brain Tissues	RI	λ_d (μm)	FWHM	T = 50 K			
				S ($\mu\text{m}/\text{RIU}$)	$Q \times 10^3$	$FoM \times 10^3$	$LoD \times 10^{-5}$
CSF	1.3333	3.2103	0.0032		1.003		
Wall of solid brain	1.3412	3.2429	0.0033	4.139241	0.982	1.250	3.99
Multi sclerosis	1.3425	3.2482	0.0035	4.130435	0.928	1.177	4.24
Oligodendroglioma	1.3531	3.2917	0.0036	4.111111	0.914	1.141	4.37
Gray matter	1.3951	3.4604	0.0043	4.048544	0.804	0.941	5.31
White matter	1.4121	3.5272	0.0047	4.022843	0.750	0.855	5.84
Low grade glioma	1.4320	3.6043	0.0053	3.992908	0.680	0.753	6.63
Medulloblastoma	1.4412	3.6394	0.0057	3.978684	0.638	0.697	7.16
Glioblastoma	1.4470	3.6617	0.0059	3.970097	0.620	0.672	7.43
Lymphoma	1.4591	3.7073	0.0064	3.952305	0.579	0.617	8.09

Finally, the comparative study shows the outcomes of our proposed work in contrast to the findings of recently published work based on 1D DPhCs for the detection of different kinds of cancerous cells in our body. This comparison has been conducted on the basis of the parameters *S*, *FoM* and *Q* as indicated in Table 5. The analysis of the data presented in Table 5 shows that the proposed design composed of SiO_2 embedded nanocomposite buffer layers of high temperature superconductor has better performance than the other configurations listed in the above table. Moreover, SiO_2 embedded nanocomposite superconducting buffer layers bring the opportunity to induce the tunability of the defect mode inside side PBG by changing the ambient temperature of nanocomposite material layers which in turn controls the performance of the design by means of improving the intensity of defect modes. The proposed design gives an opportunity to modulate defect mode and PBG both either left or right by changing θ or T , respectively.

Table 5. Comparison between performance of present work with other design on the basis of numeric values of S , Q , and FoM .

References	S (nm/RIU)	FoM (per RIU)	Q	Refractive Index Range of Analyte	Cavity Material
2018	42–43	Not mentioned	Not mentioned	1.8225–1.962801	Air cavity with metal nanocomposite
2019	2200	10^5		1.350–1.401	air cavity
2020	3081–2894	10^7	Not mentioned	1.3333–1.4833	air cavity
2021	47–68	Not mentioned	10^3	1.8225–1.962801	Graphene coated nanocomposite
2021	290	10^3	10^3	1.35–1.399	Graphene coated cavity
Proposed work	3951–4127	10^3	10^3	1.3333–1.4591	Air cavity with superconducting nanocomposite

5. Conclusions

In this manuscript, we have analyzed the externally tunable bio-sensing capabilities of the proposed 1D DPhC $(AB)^2CDC(AB)^2$ capable of detecting cancerous brain tumors in the human brain. The air cavity coated with a thin layer of SiO_2 embedded nanocomposite superconducting material has been used in the proposed 1D DPhC structure. This coating has been used to strengthen the interaction between light and fluid samples under examination. Moreover, it allows tunability of the defect mode inside the PBG of the structure by mean of change in temperature of the ambient medium of the nanocomposite layer apart from the change in angle of incidence. We have used TMM formulation and MATLAB software to obtain simulation results of the proposed work. The evaluation of the performance of the design has been conducted by calculating the sensitivity, quality factor, figure of merit and limit of detection parameters associated with the proposed work. The present work only considers the external tunability due to change in temperature as well as the angle of incidence. The tunability associated with internal parameters is beyond the scope of the present work. The maximum sensitivity which can be achieved by the proposed design is 4139.24 nm/RIU corresponding to a sample containing a wall of brain tissues with cavity layer thickness $15dd$ and $\theta = 63^\circ$ at $T = 4.5$ K. It can be marginally reduced between 4.12658 nm/RIU to 4.07594 nm/RIU by changing the temperature between 10 K to 90 K, respectively under the same sample, but the increase in the temperature improves the intensity of defect mode significantly which is one of the prime requisites in designing of any biosensor. Thus, the externally tunable bio-sensing capabilities of our design may play a significant and decisive role in the field of biomedical diagnosis. Finally, the findings of this work may be utilized for designing externally tunable biosensors composed of nanocomposite superconducting materials to monitor, detect and sense different kinds of bio-fluids with ultra enhanced sensitivity.

Author Contributions: Conceptualization, A.H.A.; methodology, A.H.A. and W.S.; software, C.M.; validation, A.H.A., C.M. and S.K.A.; formal analysis, C.M. and S.K.A.; investigation, A.H.A. and W.S. resources, Z.S.M. and N.S.A.E.-G.; data curation, A.F.A. and M.A.-D.; writing—original draft preparation, S.K.A.; writing—review and editing, A.H.A. and S.K.A.; supervision, A.H.A. and W.S.; project administration, C.M.; funding acquisition, Z.S.M., M.A.-D. and N.S.A.E.-G. All authors have read and agreed to the published version of the manuscript.

Funding: This research funded by STDF, Egypt. This paper is based upon work supported by Science, Technology & Innovation Funding Authority (STDF) under grant Post Graduate Support Grant (PGSG) under with grant number 44871.

Data Availability Statement: Not applicable.

Acknowledgments: This work was supported by the King Khalid University through a grant KCU/RCAMS/G0001-21 under the Research Center for Advance Materials (RCAMS) at King Khalid University, Saudi Arabia.

Conflicts of Interest: The authors declare that there are no conflict of interest.

References

- World Health Organization. vol. Fact Sheet No 297, (Updated 12 September 2018). Available online: <https://www.who.int/news-room/fact-sheets/detail/breast-cancer> (accessed on 21 March 2022).
- Da Silva, A.R.C. Application for predicting breast cancer through Google Prediction API. In *Escola Regional de Computação Aplicada à Saúde (ERCAS-RJ 2018)*; SBC: São Paulo, Brazil, 12–14 April 2018.
- Sayed, H.; Alamri, S.; Matar, Z.; Aly, A.H. Salinity Sensor Based on 1D Photonic Crystals by Tamm Resonance with Different Geometrical Shapes. *Plasmonics* **2022**, *17*, 409–422. [\[CrossRef\]](#)
- Ramanujam, N.R.; Amiri, I.S.; Taya, S.A.; Olyaei, S.; Udaiyakumar, R.; Pasumpon Pandian, A.; Joseph Wilson, K.S.; Mahalakshmi, P.; Yupapin, P.P. Enhanced sensitivity of cancer cell using one dimensional nano composite material coated photonic crystals. *Microsyst. Technol.* **2019**, *25*, 189–196. [\[CrossRef\]](#)
- Aly, A.H.; Zaky, Z.A. Ultra-sensitive photonic crystal cancer cells sensor with a high-quality factor. *Cryogenics* **2019**, *104*, 102991. [\[CrossRef\]](#)
- Nouman, W.M.; El-Ghany, A.; Sallam, S.M.; Dawood, A.F.; Aly, A.H. Biophotonic sensor for rapid detection of brain lesions using 1D photonic crystal. *Opt. Quantum Electron.* **2020**, *52*, 287. [\[CrossRef\]](#)
- Segovia-Chaves, F.; Yague, J.C.; Vinck-Posada, H. Effect of chemical potential and cavity thickness on defective mode sensitivity for cancer cell in a biosensor formed using a photonic crystal. *Optik* **2021**, *240*, 166823. [\[CrossRef\]](#)
- Panda, A.; Pukhrambam, P.D.; Wu, F.; Belhadj, W. Graphene-based 1D defective photonic crystal biosensor for real-time detection of cancer cell. *Eur. Phys. J. Plus* **2021**, *136*, 809. [\[CrossRef\]](#)
- Tangerman, A.; Meuwese-Arends, M.T.; van Tongeren, J.H. A new sensitive assay for measuring volatile sulphur compounds in human breath by tenax trapping and gas chromatography and its application in liver cirrhosis. *Clin. Chim. Acta* **1983**, *130*, 103–110. [\[CrossRef\]](#)
- Sun, J.; Lee, S.J.; Wu, L.; Sarntinoranont, M.; Xie, H. Refractive index measurement of acute rat brain tissue slices using optical coherence tomography. *Opt. Express* **2012**, *20*, 1084–1095. [\[CrossRef\]](#)
- Nejad, H.E.; Mir, A.; Farmani, A. Supersensitive and tunable nano-biosensor for cancer detection. *IEEE Sens. J.* **2019**, *19*, 4874–4880. [\[CrossRef\]](#)
- Zhang, Y.; Zhao, J.; Cao, J.; Mao, B. Microwave metamaterial absorber for non-destructive sensing applications of grain. *Sensors* **2018**, *18*, 1912. [\[CrossRef\]](#)
- La Spada, L.; Bilotti, F.; Vegni, L. Metamaterial biosensor for cancer detection. *IEEE Sens.* **2011**, 627–630. [\[CrossRef\]](#)
- Wu, C.J.; Liu, C.L.; Yang, T.J. Investigation photonic band structure in a one-dimensional superconducting photonic crystal. *JOSA B* **2009**, *26*, 2089–2094. [\[CrossRef\]](#)
- Yasli, A. Cancer detection with surface plasmon resonance-based photonic crystal fiber biosensor. *Plasmonics* **2021**, *16*, 1605–1612. [\[CrossRef\]](#)
- Auguie, B. Tamm Plasmon resonance in mesoporous multilayers: Toward a sensing application. *ACS Photonics* **2014**, *1*, 775–780. [\[CrossRef\]](#)
- Zaky, Z.A.; Aly, A.H. Theoretical study of a tunable low-temperature photonic crystal sensor using dielectric-superconductor nanocomposite layers. *J. Supercond. Nov. Magn.* **2020**, *33*, 2983–2990. [\[CrossRef\]](#)
- Aly, A.H.; Mohamed, D.; Zaky, Z.A.; Matar, Z.S.; Abd El-Gawaad, N.S.; Shalaby, A.S.; Tayeboun, F.; Mohaseb, M. Novel Biosensor Detection of Tuberculosis Based on Photonic Band Gap Materials. *Mater. Res.* **2021**, *24*, e20200483. [\[CrossRef\]](#)
- Bijalwan, A.; Rastogi, V. Gold-aluminum-based surface Plasmon resonance sensor with a high quality factor and figure of merit for the detection of hemoglobin. *Appl. Opt.* **2018**, *57*, 9230–9237. [\[CrossRef\]](#)
- Zaky, Z.A.; Aly, A.H. Gyroidal graphene/porous silicon array for exciting optical Tamm state as optical sensor. *Sci. Rep.* **2021**, *11*, 19389. [\[CrossRef\]](#)
- Aly, A.H.; Mohamed, D. BSCCO/SrTiO₃ One Dimensional Superconducting Photonic Crystal for Many Applications. *J. Supercond. Nov. Magn.* **2015**, *18*, 1699–1703. [\[CrossRef\]](#)
- Hsu, H.T.; Kuo, F.Y.; Wu, C.J. Optical properties of a high temperature superconductor operating in near zero-permittivity region. *J. Appl. Phys.* **2010**, *107*, 053912. [\[CrossRef\]](#)
- Upadhyay, M.; Awasthi, S.K.; Shiveshwari, L.; Shukla, S.N.; Ojha, S.P. Two channel thermally tunable band stop filter for wavelength selective switching applications by using 1D ternary superconductor photonic crystal. *J. Supercond. Nov. Magn.* **2015**, *28*, 1937–1942. [\[CrossRef\]](#)
- Upadhyay, M.; Awasthi, S.K.; Shiveshwari, L.; Srivastava, P.K.; Ojha, S.P. Thermally tunable photonic filter for WDM networks using 1D superconductor dielectric photonic crystals. *J. Supercond. Nov. Magn.* **2015**, *28*, 2275–2280. [\[CrossRef\]](#)
- Aly, A.H.; Awasthi, S.K.; Mohaseb, M.A.; Matar, Z.S.; Amin, A.F. MATLAB Simulation-Based Theoretical Study for Detection of a Wide Range of Pathogens Using 1D Defective Photonic Structure. *Crystals* **2022**, *12*, 220. [\[CrossRef\]](#)
- YaVetrov, S.; Avdeeva, A.Y.; Timofeev, I.V. Spectral properties of a one-dimensional photonic crystal with a resonant defect nanocomposite layer. *J. Exp. Theor. Phys.* **2011**, *113*, 755–761. [\[CrossRef\]](#)
- Born, M.; Wolf, E. Basic properties of the electromagnetic field. *Princ. Opt.* **1980**, *44*, 1–70.

28. Awasthi, S.K.; Malaviya, U.; Ojha, S.P. Enhancement of omnidirectional total reflection wavelength range by using one-dimensional ternary photonic bandgap material. *JOSA B* **2006**, *23*, 2566–2571. [[CrossRef](#)]
29. Awasthi, S.K.; Malaviya, U.; Ojha, S.P. Enhancement of omnidirectional high-reflection wavelength range in 1D ternary periodic structures: A comparative study. *J. Nanophotonics* **2008**, *2*, 023505.
30. Zaky, Z.A.; Panda, A.; Pukhrambam, P.D.; Aly, A.H. The impact of magnetized cold plasma and its various properties in sensing applications. *Sci. Rep.* **2022**, *12*, 3754. [[CrossRef](#)]
31. Biswas, T.; Luu, T. In vivo MR Measurement of Refractive Index, Relative Water Content and T2 Relaxation time of Various Brain lesions With Clinical Application to Discriminate Brain Lesions. *Internet J. Radiol.* **2009**, *13*, 1–9.
32. Aly, A.H.; Awasthi, S.K.; Mohamed, A.M.; Al-Dossari, M.; Matar, Z.S.; Mohaseb, M.A.; El-Gawaad, N.S.A.; Amin, A.F. 1D reconfigurable bistable photonic device composed of phase change material for detection of reproductive female hormones. *Phys. Scr.* **2021**, *96*, 125533. [[CrossRef](#)]
33. Aly, A.H.; Awasthi, S.K.; Mohamed, A.M.; Matar, Z.S.; Mohaseb, M.A.; Al-Dossari, M.; Tammam, M.T.; Zaky, Z.A.; Amin, A.F.; Sabra, W. Detection of Reproductive Hormones in Females by Using 1D Photonic Crystal-Based Simple Reconfigurable Biosensing Design. *Crystals* **2021**, *12*, 1533. [[CrossRef](#)]